Science and Technology Indonesia
e-ISSN:2580-4391 *p*-ISSN:2580-4405
Vol. 11, No. 3, July 2026

Research Paper

Effect of Deformation by Wire Drawing on the Mechanical and Electrical Properties of Aluminum

Lazhar Yahia[1,2*], Fatima Zohra Benlahreche[3], Wahid Kaddouri[4], Elamine Nouicer[5], Sihem Abderrahmane[2], Lyamine Briki[6], Mosbah Zidani[7]

[1]*Department of Electromechanical Engineering, Faculty of Technology, University of Batna 2, Batna, 05000, Algeria*
[2]*Surface Engineering Laboratory, Department of Chemistry, Faculty of Sciences, University of Annaba, Annaba, 23000, Algeria*
[3]*Department of Chemical Engineering, Faculty of Process Engineering, University of Constantine 3, Constantine, 25000, Algeria*
[4]*Structural Mechanics and Materials Laboratory, Department of Mechanical Engineering, Faculty of technology, University of Batna 2, Batna, 05000, Algeria*
[5]*Department of Physics, Faculty of Sciences, University of Constantine 1, Constantine, 25000, Algeria*
[6]*Department of Civil Engineering, Faculty of Technology, University of Batna 2, Batna, 05000, Algeria*
[7]*Department of Science and Technology, Faculty of Technology, University of Batna 2, Batna, 05000, Algeria*
*__Corresponding author__: l.yahia@univ-batna2.dz

Abstract
This research investigates the influence of cold wire drawing on the electromechanical properties of high-purity (99.7%) aluminum conductors. Aluminum wires were subjected to progressive plastic deformation, with cross-sectional reduction rates ranging from 11.25% to 88.44%. The results demonstrate that mechanical deformation significantly enhances the ultimate tensile strength, reaching a peak value of 116.14 MPa and a Vickers hardness of 57.63 HV at the maximum reduction rate. Conversely, a marked reduction in elongation at break was observed, indicating a loss of ductility due to intense work hardening. Regarding electrical performance, the study reveals that electrical resistivity increases by only 0.87% over the full deformation range, while electrical conductivity exhibits a proportional decline. This degradation in transport properties is physically attributed to the increased density of lattice defects (dislocations) acting as electron scattering centers. These findings highlight the critical trade-off between mechanical reinforcement and electrical efficiency, providing essential data for the optimization of high-performance conductors for power transmission.

Keywords
Aluminum 99.7%, Cold Wire Drawing, Microhardness, Ultimate Tensile Strength, Conductivity, Resistivity

Received: 3 January 2026, Accepted: 31 March 2026
https://doi.org/10.26554/sti.2026.11.3.894-902

1. INTRODUCTION

Aluminum (Al) has established itself as a cornerstone material in modern electrical engineering, playing a strategic role in the deployment of global power transmission infrastructures. While silver, copper, and gold exhibit higher absolute conductivities (Caruso and Ambrogio, 2021; Omeje, 2020), aluminum's superior strength-to-weight ratio and cost-efficiency make it the preferred candidate for long-distance overhead lines and large-scale infrastructure. This preference is fundamentally driven by its low density and the presence of highly mobile valence electrons, which ensure efficient charge transport in weight-sensitive applications (Kiessling et al., 2003; Riba et al., 2020). Over the past several decades, the application of aluminum has evolved from basic household wiring to sophisticated industrial conductors designed for extreme operational environments (Reinke et al., 2020). However, the practical performance of aluminum is often constrained by impurities, alloying elements, and the formation of a natural oxide layer (Czerwinski, 2024).

The mechanical and electrical properties of aluminum are critical factors determining its suitability for electrical conductors (Parvizi et al., 2025). In the context of wire manufacturing, the material must undergo intense plastic deformation to achieve the geometric dimensions and mechanical specifications dictated by international standards. This cold wire drawing process reconfigures the metal's internal crystalline structure through combined tension and compression (Caruso and Ambrogio, 2021). During this process, electrical resistivity and thermal conductivity are significantly influenced by microstructural evolution (Brandt and Neuer, 2007; Lunn and Apelian, 2024). Furthermore, advanced processing techniques, such as the combined drawing of aluminum alloys with rare earth additives, have been explored to enhance these semi-finished products (Bespalov et al., 2024).

A significant body of literature has explored the deformation of aluminum and its alloys, focusing primarily on metallurgical mechanisms such as microstructural evolution and precipitation kinetics, particularly in 6xxx series alloys (Allamki et al., 2023; Cui et al., 2017; Zhu et al., 2018). Several researchers have analyzed these parameters in isolation, focusing either on mechanical strengthening through work hardening (Hou et al., 2015; Luo et al., 2017) or on electrical conductivity (Chen et al., 2019). While drawing is essential for increasing yield strength and hardness, it simultaneously introduces a critical density of dislocations and lattice distortions that act as scattering centers for electrons (Balogun et al., 2007). Despite these advancements, there is a notable scarcity of research comprehensively addressing the synergetic relationship between mechanical reinforcement and electrical properties during the cold-drawing process. Limited studies have focused on the coupled electro-mechanical response under extreme reduction rates, especially for high-purity (99.7%) grades. Most existing studies do not fully capture the critical trade-off occurring during high-strain processing above 80% reduction.

Therefore, this research intends to bridge this knowledge gap by investigating the coupled electro-mechanical behavior of high-purity aluminum wires under severe cold-drawing conditions. This study focuses on establishing a direct correlation between high cross-sectional reduction rates (up to 88.44%) and the concurrent evolution of ultimate tensile strength, Vickers hardness, electrical resistivity, and conductivity. The objectives of this research are to determine the physical impact of dislocation density on electron transport and to provide an integrated framework for optimizing plastic deformation in high-voltage conductor manufacturing.

2. EXPERIMENTAL SECTION

2.1 Materials

The material investigated in this study consists of high-purity aluminum conductors supplied by the Cable Industry Company (ENICAB, Biskra, Algeria). The samples were provided as continuous cylindrical coils with an initial diameter of 8 mm. The material is characterized by a high aluminum content (99.70% Al), representing an electrical conductor (EC) grade of near-intrinsic purity. The detailed chemical composition of the studied aluminum is presented in Table 1.

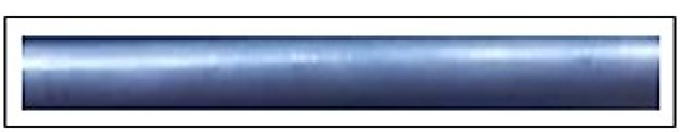

Figure 1. Aluminum Wire

With a nominal purity of 99.70%, this material is classified as electrical conductor (EC) grade. In this high-purity system, the presence of Fe (0.250%) and Si (0.100%) primarily leads to the formation of fine intermetallic precipitates, which have a limited impact on electron scattering compared to elements in solid solution (Czerwinski, 2024; Lunn and Apelian, 2024). Notably, trace amounts of elements such as Ti, V, and Cr are strictly controlled, as these are known to significantly degrade electrical conductivity even at low concentrations (Subedi et al., 2022). The inclusion of B (0.050%) is strategically important, as it helps sequester these transition metals into stable borides, ensuring the material maintains its superior electrical performance during subsequent processing (Parvizi et al., 2025). The representative geometry of the starting material is illustrated in Figure 1.

2.2 Methods

2.2.1 Sample Preparation and Surface Treatment

To ensure the reliability of subsequent mechanical and electrical characterizations, a rigorous surface preparation protocol was implemented to eliminate exogenous contaminants. Prior to cold-drawing and analytical testing, the aluminum rods underwent a systematic multi-step cleaning procedure at room temperature. The process began with chemical degreasing, where specimens were cleaned using high-purity acetone to dissolve residual lubricants, oils, and organic contaminants from industrial handling. Following degreasing, the rods were thoroughly rinsed with distilled water to neutralize the surface and remove solvent traces. Finally, the wires were dehydrated using a high-pressure forced-air system. This standardized preparation was essential to prevent surface artifacts from influencing contact resistance during electrical measurements or initiating premature failure during tensile testing. All prepared samples were stored in a controlled environment to maintain surface integrity and minimize the thickening of the natural oxide layer prior to processing.

2.2.2 Vickers Microhardness

Vickers microhardness measurements were performed to quantify the mechanical reinforcement and strain-hardening distribution induced by the cold-drawing process. The tests were conducted at ambient temperature using an HVS-1000Z digital microhardness tester equipped with a standard diamond pyramidal indenter. A constant load of 0.2 kgf (1.96 N) was applied with a dwell time of 15 s, ensuring stable and well-defined indentation profiles. To ensure statistical reliability and evaluate the homogeneity of the mechanical properties, characterization was carried out on the longitudinal sections of the specimens. Each sample was carefully prepared and polished to a mirror finish prior to testing. For each reduction rate, five independent indentations were recorded at regular intervals. This longitudinal profiling is essential for assessing the impact of severe plastic deformation on the material's local hardness. The average values and corresponding standard deviations were calculated to provide a comprehensive representation of the hardness evolution as a function of the drawing strain.

Table 1. Chemical Composition of Aluminum (%)

Si	Fe	Cu	Mn	Mg	Cr	Zn	Ti	B	Ga	V	Na	Al
0.100	0.250	0.050	0.010	0.030	0.010	0,050	0.010	0.050	0.030	0.010	0.030	99.70

2.2.3 Wire Drawing Operation

The wire drawing process investigated in this study was performed using as-received aluminum wire rods with an initial nominal diameter of d=8mm procured directly from the industrial coils at ENICAB. To analyze the progressive impact of plastic deformation, specimens were systematically extracted at various stages along the continuous drawing line, following the series of cross-sectional transformations. During the drawing sequence, the wire surface was meticulously lubricated to counteract the intense frictional forces generated at the wire-die interface. Although the process begins at ambient temperature, the adiabatic heating resulting from rapid plastic deformation and friction necessitates effective lubrication to maintain a smooth surface finish and prevent thermal-induced softening. The intensity of the cold-working process is traditionally expressed by the reduction in area, which serves as a metric for the degree of strain hardening. To ensure clarity in the strain evolution analysis, the reduction rate was defined as the ratio of the change in cross-sectional area to the initial area. As emphasized by Volokitin et al. (2021), the distinction between initial (S0) and final (Sf) cross-sections is critical for accurate modeling; therefore, the deformation rate was calculated according to the Equation (1):

$$e\% = \frac{S_0 - S_f}{S_0} \times 100 \tag{1}$$

This systematic approach allowed for the characterization of the material across eight distinct reduction levels, ranging from 0% (as-received) to a severe deformation of 88.44%, providing a comprehensive overview of the electro-mechanical performance spectrum. The resulting drawn wires exhibited cumulative reduction of area rates of 11.25%, 38.27%, 53.18%, 65.13%, 72.85%, 80.36%, and 88.44%. The visual evolution of these wire geometries is shown in Figure 2. Subsequent to the drawing stages, the wires were sectioned into standardized specimens for mechanical characterization. To prevent any adiabatic recovery or unintentional annealing that could compromise the work-hardened state, the samples were manually cut using a precision hacksaw at a controlled low speed under a continuous distilled water coolant stream. This methodology ensured the thermal stability of the microstructure during preparation. Each tensile test specimen was prepared with a standardized gauge length of L0=30 cm, adhering to international protocols for electrical conductor testing.

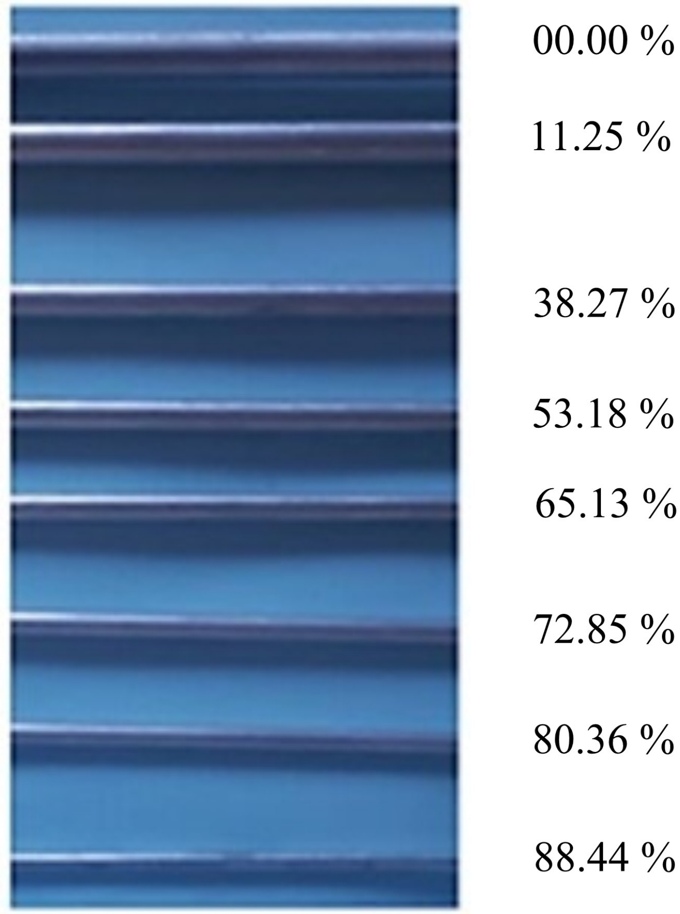

Figure 2. Rate Reduction of Aluminum Wires

2.2.4 Tensile Testing

Uniaxial tensile tests were performed to analyze the mechanical behavior of aluminum wires subjected to various reduction rates during the drawing process. This characterization is essential for determining critical mechanical properties such as yield strength, ultimate tensile strength, fracture stress, and elongation at break. The experiments were conducted at the ENICAB laboratory using a Zwick universal testing machine at ambient temperature. In accordance with ISO 6892 standards, specimens were tested at a constant crosshead speed of 5 mm/min until failure. This controlled strain rate ensures quasi-static loading conditions, enabling the acquisition of precise stress-strain curves that reflect the material's work-hardened state. The investigated wires featured reduction rates of 0%, 11.25%, 38.27%, 53.18%, 65.13%, 72.85%, 80.36%, and 88.44%. Prior to testing, all specimens were meticulously polished to a 1200 grit finish to eliminate surface imperfections that could act as stress concentrators. The resulting data are fundamental for evaluating the quality and mechanical behavior of aluminum conductors, particularly for high-demand applications within the electrical power industry.

2.2.5 Electrical Resistivity Testing

Electrical resistivity testing of 99.7% Al conductor wires is a critical stage in ensuring both the quality and safety of the final electrical cables, verifying compliance with international standards and technical specifications. Measurements were performed at ambient temperature in the ENICAB laboratory using a high-precision Resistomat type 2303 micro-ohmmeter. For accurate data acquisition, the specimens were prepared with a total length of 1.20 m, exceeding the bridge dimensions to ensure secure clamping between the terminals. The measurement protocol involved injecting a stabilized current through a calibrated 1 m gauge length. Crucially, maintaining a constant clamping force at the jaws is essential to break the natural aluminum oxide layer, which acts as an insulator, thereby ensuring low contact resistance and high measurement reproducibility. This setup allows for the precise determination of the material's intrinsic electrical properties as a function of the cold-drawing strain. All resistivity data were recorded under controlled environmental conditions to minimize thermal fluctuations, ensuring the accuracy of the transport property characterization.

3. RESULTS AND DISCUSSION

3.1 Mechanical Properties

3.1.1 Microhardness Measurement

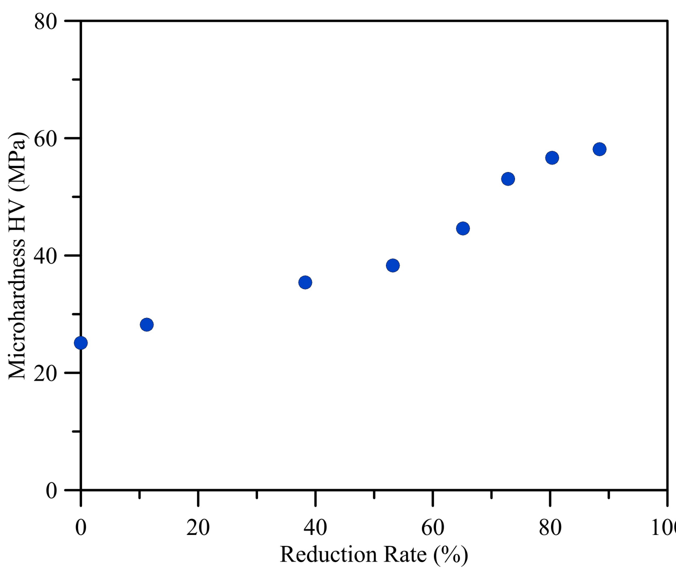

Figure 3. Evolution of Microhardness as a Function of the Reduction Rate for Al.

The evolution of Vickers microhardness as a function of the reduction rate is illustrated in Figure 3. The experimental data reveal a monotonic increase in microhardness values, directly proportional to the cross-sectional reduction rate. This hardening behavior is a macroscopic manifestation of strain hardening induced during the cold-drawing process (Hou et al., 2015). At the microscopic scale, this strengthening is governed by the accumulation and interaction of lattice defects. Continuous plastic deformation triggers a significant increase in dislocation density and the generation of point defects, such as vacancies and interstitials (Chen et al., 2019). These defects act as barriers to dislocation motion, a phenomenon known as dislocation forest hardening, which reduces the mean free path of mobile dislocations and subsequently enhances the material's flow stress and hardness.

Furthermore, the microhardness profile across the wire cross-section serves as a critical diagnostic tool for assessing process consistency. While the observed upward trend confirms effective strengthening, the uniformity of these values suggests a homogeneous distribution of plastic strain across the reduction levels. Any localized fluctuations would otherwise indicate the presence of residual stresses or microstructural in homogeneities, such as shear bands, which are typical of non-uniform deformation during the drawing stages (Zisman et al., 2006).

3.1.2 Effect of Tensile Deformation on the Mechanical Properties of Aluminum

Mechanical response of the aluminum conductor under uniaxial tension was evaluated to quantify the impact of the drawing process. The key mechanical parameters, including yield strength (YS), ultimate tensile strength (UTS), and elongation at break, are summarized in Table 2.

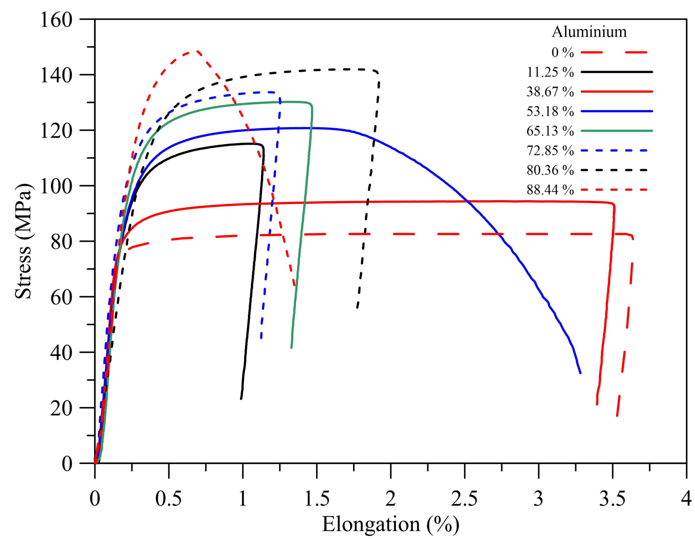

Figure 4. Stress-Strain Curves of Al at Various Reduction Rates

To evaluate these properties, a series of uniaxial tensile tests was conducted under quasi-static loading conditions at a constant strain rate. The resulting engineering stress-strain behavior is illustrated in Table 2 and Figure 4, which displays the superposition of the characteristic curves for the various reduction rates investigated.

Table 2. Summary of the Mechanical Properties of Al at Different Reduction Rates

Mechanical Characteristics	Reduction Rate (%)							
	00.00	11.25	38.27	53.18	65.13	72.85	80.36	88.44
Yield strength (MPa)	65.13	72.21	83.11	96.22	102.65	107.41	111.33	116.14
Ultimate tensile strength (MPa)	80	90	110.51	118.72	128.13	132.22	141.44	150.32
Breaking strength (MPa)	11.13	22.14	28.32	65.89	45.21	48.33	52.12	60.02
Elongation at break (%)	3.48	3.32	2.63	2.46	1.25	1.01	0.86	0.77

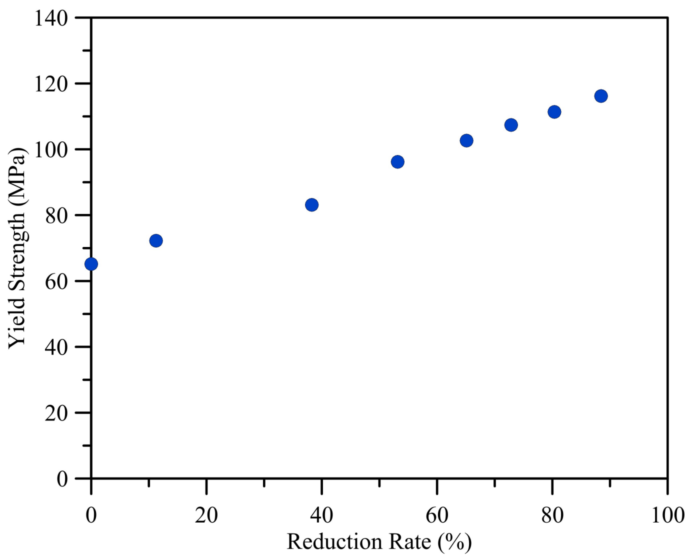

Figure 5. Evolution of the Yield Strength as a Function of the Reduction Rate for Al

The tensile response of the 99.7% Al wires across various reduction rates is illustrated in Figures 5 to 7. The experimental data reveal a significant transition in deformation mechanisms where a substantial increase in yield strength is shown in Figure 5 and a concomitant decrease in elongation is observed in Figure 6; both parameters are summarized in Table 2. This antagonistic evolution is a primary manifestation of the strain hardening effect induced during the cold-drawing process (Volokitin et al., 2021). At low deformation levels (0% and 11.25%), the aluminum exhibits characteristically ductile behavior with extensive plastic flow and pronounced necking prior to failure. This regime, typical of the annealed or near-annealed state, indicates a high energy absorption capacity. As the reduction rate progresses through intermediate values (38.27% to 65.13%) toward the highest levels (72.85% to 88.44%), the material reaches a hard-drawn state. In this stage, continuous plastic deformation leads to a saturation of the work-hardening capacity, characterized by minimal residual elongation and rapid fracture.

Although direct metallographic observations were not conducted in this study, these macroscopic mechanical results provide a robust basis for a phenomenological analysis of the microstructure. The observed correlation between the reduction rate and the increase in flow stress is consistent with the Taylor hardening model (Hou et al., 2015), where the accumulation and entanglement of dislocations act as the primary strengthening mechanism. This transition is intrinsically linked to two well-documented phenomena in FCC metals such as 99.7% Al.

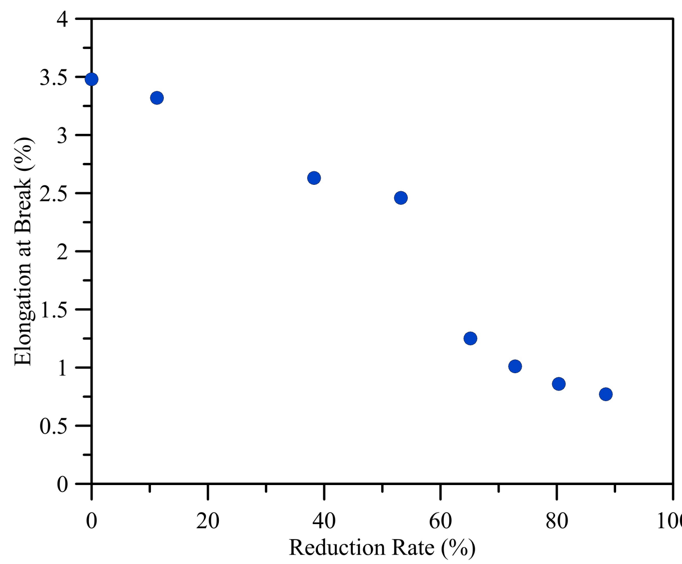

Figure 6. Evolution of Elongation as a Function of the Reduction Rate for Al

First, the grain refinement and elongation occurring at high reduction rates inevitably lead to the development of a fibrous microstructure, where grains are elongated along the drawing axis. This reduction in the transverse grain dimension contributes to the material's strengthening via the Hall-Petch effect at the subgrain level (Chen et al., 2019). Second, the dislocation density evolution, evidenced by the loss of ductility as shown in Figures 6 and 7, serves as indirect proof of dislocation multiplication. These defects impede further lattice slip, thereby increasing the mechanical load required to initiate fracture. Hardening ensures that the drawn wires fulfill the rigorous breaking-load specifications required for high-tension electrical conductors produced at ENICAB (Volokitin et al., 2021).

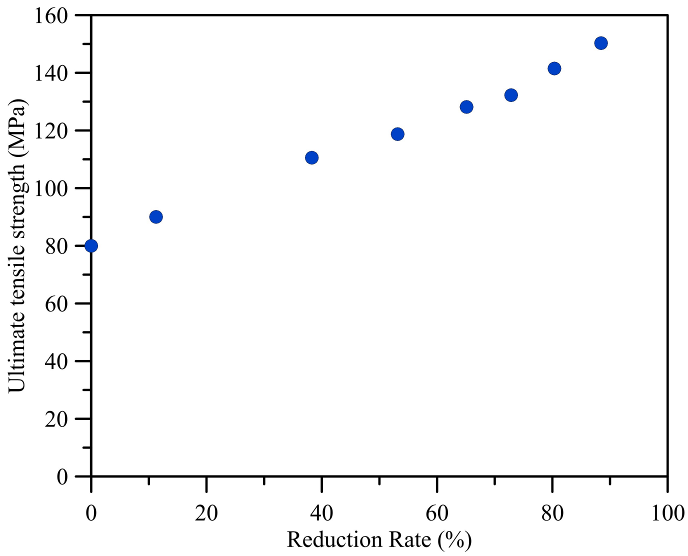

Figure 7. Evolution of the Ultimate Tensile Strength as a Function of the Reduction Rate for Al

Table 3. Electrical Resistivity and Conductivity Parameters of Al Wires at Various Reduction Rates

Reduction Rate [%]	Electrical Properties	
	Electrical Resistivity ($\Omega mm^2/m$)	Electrical Conductivity ($m/\Omega mm^2$)
As received (00.00)	$0.02761^{\pm 0.00034}$	$36.22^{\pm 0.44}$
11.25	$0.02763^{\pm 0.00037}$	$36.19^{\pm 0.45}$
38.27	$0.02768^{\pm 0.00034}$	$36.13^{\pm 0.49}$
53.18	$0.02771^{\pm 0.00034}$	$36.09^{\pm 0.45}$
65.13	$0.02775^{\pm 0.00034}$	$36.04^{\pm 0.44}$
72.85	$0.02778^{\pm 0.00038}$	$36.01^{\pm 0.44}$
80.36	$0.02782^{\pm 0.00036}$	$35.95^{\pm 0.48}$
88.44	$0.02785^{\pm 0.00037}$	$35.91^{\pm 0.47}$

3.2 Electrical Properties

3.2.1 Resistivity Measurement and Analysis

The electrical properties of the Al wires, characterized as a function of the reduction rate, are summarized in Table 3. Resistivity uncertainty calculation for Al as-received:

The electrical resistivity is defined in Equation (2):

$$\rho = \frac{RA}{L} = \frac{R\pi d^2}{4L} \quad (2)$$

Where R is the resistance, d the wire diameter, and L the gauge length. According to the propagation of uncertainty theory, the fractional uncertainty in resistivity ρ is expressed by Equation (3):

$$\frac{\Delta\rho}{\rho} = \sqrt{\left(\frac{\Delta R}{R}\right)^2 + 2\left(\frac{\Delta d}{d}\right)^2 + \left(\frac{\Delta L}{L}\right)^2} \quad (3)$$

Using the experimental precision of the instruments, $R = 549 \pm 0.006$ (mΩ), length $L = 1 \pm 0.002$ (m) and diameter $d = 8 \pm 0.02$ (mm). The relative uncertainties are calculated as follows:

$$\frac{\Delta R}{R} = \frac{0.006}{549} = 0.010929, \quad 2\left(\frac{\Delta d}{d}\right) = 2\frac{0.02}{8} = 0.005, \quad \frac{\Delta L}{L} = \frac{0.002}{1} = 0.002$$

The total relative uncertainty is then calculated as follows:

$$\frac{\Delta\rho}{\rho} = \sqrt{(0.010929)^2 + (0.005)^2 + (0.002)^2} = 0.01218 = 1.22\%$$

For a resistivity value of $\rho = 0.02761$ ($\Omega mm^2/m$), the absolute uncertainty $\Delta\rho$ is derived from the measured value:

$$\Delta\rho = 0.02761 \times 0.01218 = 0.00034 \ (\Omega mm^2/m)$$

The absolute uncertainty is derived from the measured value. For the as-received aluminum wire:

$$\rho = 0.02761 \pm 0.00034 \ (\Omega mm^2/m)$$

Conductivity uncertainty calculation for Al as-received:

The electrical conductivity is defined by the following relationship in Equation (4):

$$\sigma = \frac{1}{\rho} = \frac{4L}{R\pi d^2} \quad (4)$$

For the electrical conductivity, the fractional uncertainty is identical to that of resistivity, as shown in Equation (5).

$$\frac{\Delta\sigma}{\sigma} = \frac{\Delta\rho}{\rho} \quad (5)$$

The calculated value of electrical conductivity is $\sigma = 36.2187$ ($m/\Omega mm^2$). The absolute uncertainty is derived from the results of Equation (5), giving $\Delta\sigma = 0.441$ ($m/\Omega mm^2$).

Therefore, the final conductivity is expressed as:

$$\sigma = 36.2187^{\pm 0.441} \ (m/\Omega mm^2)$$

As summarized in Table 3 and shown in Figure 8, the experimental data indicate a slight, monotonic increase in resistivity as the reduction rate progresses, although the values remain relatively stable. While the decrease in wire diameter naturally leads to an increase in total electrical resistance (R), the intrinsic resistivity (ρ) is governed by the microstructural state of the 99.7% Al conductor. The experimental data in Table 3 shows a progressive increase in electrical resistivity, rising from 0.02761 to 0.02785 (Ωmm^2/m), which represents a total increase of 0.87% at the maximum reduction rate. Conversely, electrical conductivity slightly declines from 36.22 to 35.91 (m/Ωmm^2). This low degradation (less than 1%) in transport properties, despite the significant mechanical strengthening to 116.14 (MPa), indicates that the electron scattering induced by the high density of dislocations and lattice defects remains within industrially acceptable limits for high-purity aluminum (99.7%). It is well-established that a work-hardened metal exhibits reduced electrical conductivity compared to its annealed state.

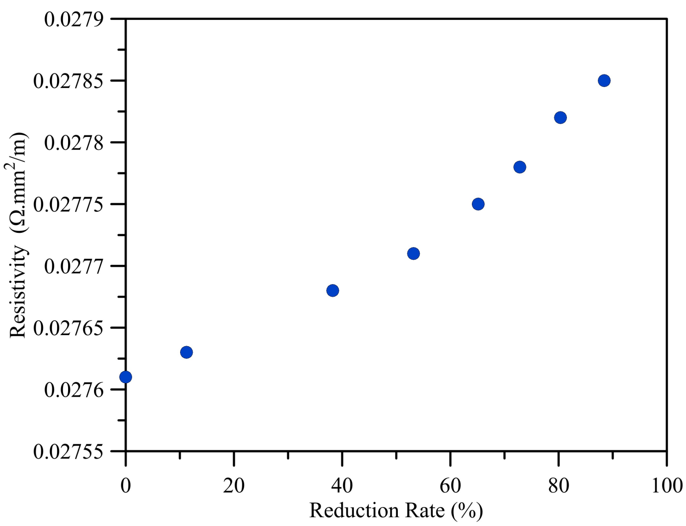

Figure 8. Evolution of Resistivity as a Function of the Reduction Rate for Al

The Figure 8 represents the variation of the electrical resistivity of aluminum wires as a function of reduction rate. This phenomenon is attributed to the increase in lattice entropy and structural disorder induced by the drawing process. According to Matthiessen's Rule Alley and Serin (1959); Balogun et al. (2007), the total resistivity of a metal is the sum of contributions from thermal vibrations (phonons) and structural defects. In the present study, the reduction rate applied during drawing generates a high density of dislocations, vacancies, and grain boundaries. These defects act as scattering centers for conduction electrons, effectively reducing their mean free path and increasing the overall resistivity (Chen et al., 2019; Çetinarslan, 2009; Koprowski et al., 2020; Zisman et al., 2006). The relative stability of the resistivity, despite the high reduction rates, can be explained by the high purity (99.7%) of the aluminum used. In such high-purity systems, the contribution of solute atoms to electron scattering is minimal, leaving the dislocation density as the primary variable. Furthermore, according to the free-electron theory, the electrical conductivity, defined as the ratio of current density to electric field strength, is directly dependent on the mobility of charge carriers. As the reduction rate intensifies, the probability of electron–defect scattering increases, which inversely impacts the material's ability to carry current.

These results confirm that while significant mechanical strengthening is achieved, the electrical performance remains within standardized limits for 1350-grade aluminum conductors (Caruso and Ambrogio, 2021). Lattice defects and electron scattering: an interaction of electrons with lattice and structural defects leads to scattering of electron waves and an increase in the electrical resistivity. In a metal lattice, point defects such as vacancies, self-interstitials and atomic impurities; linear defects as dislocation lines and dislocation loops; and planar defects as stacking faults, grain boundaries and crystal surfaces act as scattering sites. According to the Matthiessen's rule Alley and Serin (1959), the total electrical resistivity of metals (ρ) is affected by their metal lattice (ρ_t) and structural disorder caused by impurities (ρ_{imp}) and deformation (ρ_{def}), as shown in Equation (6):

$$\rho = \rho_t + \rho_{imp} + \rho_{def} \tag{6}$$

In this case, annealing the work-hardened material is necessary because it eliminates these defects, resulting in a gradual decrease in the wire's resistivity.

3.2.2 Conductivity Measurement and Analysis

The electrical conductivity measurements of 99.7% Al wires as a function of the reduction rate are summarized in Table 3. The experimental correlation between these parameters is further illustrated in Figure 9. A clear downward trend is observed, where the electrical conductivity decreases monotonically as the degree of plastic deformation intensifies during the wire drawing process (Subedi et al., 2022). This degradation in conductivity is a direct consequence of the microstructural evolution induced by strain hardening. According to the semi-classical model of metallic conduction, the movement of charge carriers is governed by the periodicity of the crystal lattice. However, the wire drawing process introduces a high density of structural defects, including dislocation tangles, vacancies, and grain boundaries, which act as scattering centers (Czerwinski, 2024; Alley and Serin, 1959; Koprowski et al., 2020). As the reduction rate increases, several mechanisms impede electron flow. First, lattice distortion caused by cold working leads to significant disruption of the aluminum lattice, increasing the entropy of the system and disrupting the periodic potential required for coherent electron transport. Second, dislocation-induced impedance arises from the proliferation of dislocations, which reduces the mean free path of electrons.

Each encounter between a conduction electron and a dislocation results in a scattering event, which macroscopically manifests as an increase in resistivity and a concomitant loss in

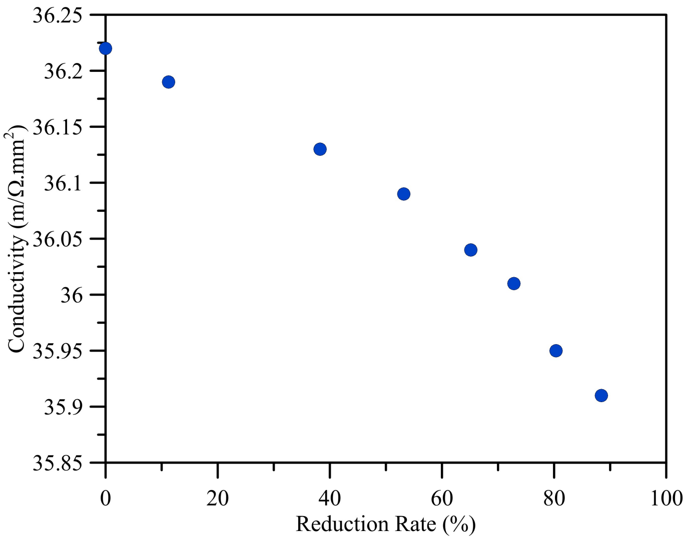

Figure 9. Evolution of Conductivity as a Function of the Reduction Rate for Al

conductivity. Finally, interfacial scattering occurs as the refinement of the grain structure increases the density of grain boundaries per unit volume, further hindering the passage of electric current. Despite these effects, the high purity (99.7%) of the Al conductor ensures that the conductivity remains within the tolerances required for industrial applications. These results demonstrate that while the mechanical properties are optimized through reduction rate control, the electrical performance is slightly compromised due to the inherent increase in electron-defect interactions (Murashkin et al., 2015; Belov et al., 2020; Medvedev et al., 2022).

4. CONCLUSIONS

This study systematically investigated the evolution of the electromechanical properties of industrial-grade 99.7% Al conductors under various cold-drawing reduction rates. The results demonstrate that cold-drawing induces a profound enhancement in mechanical durability, where the Vickers microhardness increased from 26.03 HV to a peak of 57.63 HV at an 88.44% reduction rate, while the ultimate tensile strength nearly doubled to reach 116.14 MPa. Regarding electrical performance, the properties exhibited a clear sensitivity to plastic deformation; specifically, while electrical resistivity slightly increased from 0.02761 to 0.02785 ($\Omega\,\mathrm{mm}^2/\mathrm{m}$), the electrical conductivity experienced a corresponding decrease due to the accumulation of structural defects. However, this degradation remained minimal at 0.87% relative to the significant mechanical gains, confirming high energy efficiency for high-voltage transmission. These findings validate the industrial manufacturing protocols at ENICAB and provide a robust scientific framework for optimizing the load-bearing capacity of aluminum wires while maintaining superior electrical performance. Future research should focus on the impact of microstructural recovery during long-term operational heating to further advance the reliability of high-performance conductors.

5. ACKNOWLEDGMENT

The authors would like to express their deepest gratitude to the management and the entire staff of ENICAB (Biskra, Algeria) for their invaluable assistance and for providing the necessary facilities to conduct this research. Special thanks are extended to the laboratory team for their technical expertise and support during the preparation and characterization of the aluminum wire specimens. Their constant encouragement and professional guidance significantly contributed to the success of this project on high-voltage electrical conductors.

REFERENCES

Allamki, A., M. Al-Maharbi, S. Z. Qamar, and F. Al-Jahwari (2023). Precipitation Hardening of the Electrical Conductor Aluminum Alloy 6201. *Metals*, **13**(6); 1111

Alley, P. and B. Serin (1959). Deviations from Matthiessen's Rule in Aluminum, Tin, and Copper Alloys. *Physical Review*, **116**(2); 334–338

Balogun, S. A., D. E. Esezobor, and S. O. Adeosun (2007). Effects of Deformation Processing on the Mechanical Properties of Aluminum Alloy 6063. *Metallurgical and Materials Transactions A*, **38**(7); 1570–1574

Belov, N., M. Murashkin, N. Korotkova, T. Akopyan, and V. Timofeev (2020). Structure and Properties of Al–0.6wt.%Zr Wire Alloy Manufactured by Direct Drawing of Electromagnetically Cast Wire Rod. *Metals*, **10**(6); 769

Bespalov, V. M., D. S. Voroshilov, V. A. Berngardt, S. B. Sidelnikov, and I. L. Konstantinov (2024). Influence of the Parameters of Combined Processing and Drawing on the Structure and Properties of Conductor Semi-Finished Products. *Metals and Materials International*, **30**(3); 773–799

Brandt, R. and G. Neuer (2007). Electrical Resistivity and Thermal Conductivity of Pure Aluminum and Aluminum Alloys. *International Journal of Thermophysics*, **28**(5); 1429–1446

Caruso, S. and G. Ambrogio (2021). Novel Drawing System Approach to Manufacture Performant Commercially Pure Aluminium Fine Wires. *The International Journal of Advanced Manufacturing Technology*, **117**(3); 883–895

Çetinarslan, C. S. (2009). Effect of Cold Plastic Deformation on Electrical Conductivity of Various Materials. *Materials & Design*, **30**(3); 671–673

Chen, X., G. S. Huang, S. S. Liu, T. Z. Han, B. Jiang, A. T. Tang, and F. S. Pan (2019). Grain Refinement and Mechanical Properties of Pure Aluminum Processed by Accumulative Extrusion Bonding. *Transactions of Nonferrous Metals Society of China*, **29**(3); 437–447

Cui, X., Y. Wu, G. Zhang, Y. Liu, and X. Liu (2017). Study on the Improvement of Electrical Conductivity and Mechanical Properties of Low Alloying Electrical Aluminum Alloys. *Composites Part B: Engineering*, **110**; 130–137

Czerwinski, F. (2024). Aluminum Alloys for Electrical Engineering: A Review. *Journal of Materials Science*, **59**(31); 14847–14892

Hou, J. P., Q. Wang, H. J. Yang, X. M. Wu, C. H. Li, X. W. Li, and Z. F. Zhang (2015). Microstructure Evolution and Strengthening Mechanisms of Cold-Drawn Commercially Pure Aluminum Wire. *Materials Science and Engineering: A*, **639**; 103–106

Kiessling, F., P. Nefzger, U. Kaintzyk, and J. F. Nolasco (2003). *Overhead Power Lines: Planning, Design, Construction*. Springer, Berlin, Germany

Koprowski, P., M. Lech-Grega, Ł. Wodziński, B. Augustyn, S. Boczkal, M. Ożóg, and W. Szymański (2020). The Effect of Low Content Additives on Strength, Resistivity and Microstructural Changes in Wire Drawing of 1xxx Series Aluminium Alloys for Electrical Purposes. *Materials Today Communications*, **24**; 101039

Lunn, K. F. and D. Apelian (2024). Thermal and Electrical Conductivity of Aluminum Alloys. *Materials Science and Engineering: A*, **924**; 147766

Luo, X. M., Z. M. Song, M. L. Li, Q. Wang, and G. P. Zhang (2017). Microstructural Evolution and Service Performance of Cold-Drawn Pure Aluminum Conductor Wires. *Journal of Materials Science & Technology*, **33**(9); 1039–1043

Medvedev, A. E., M. Y. Murashkin, N. A. Enikeev, and R. Z. Valiev (2022). Mechanical Properties and Electrical Conductivity of Al–Fe Alloys. *Frontiers in Materials Technologies*, **3**(1); 96–105

Murashkin, M., A. Medvedev, V. Kazykhanov, A. Krokhin, G. Raab, N. Enikeev, and R. Z. Valiev (2015). Enhanced Mechanical Properties and Electrical Conductivity in Ultrafine-Grained Al 6101 Alloy Processed via ECAP-Conform. *Metals*, **5**(4); 2148–2164

Omeje, C. O. (2020). Corona Loss Minimization on High Voltage Transmission Line Network Using Bundled Conductors. *International Journal of Engineering and Advanced Technology*, **9**(3); 1545–1550

Parvizi, P., S. Karabay, M. Erdem, and S. Altintas (2025). Mechanical and Physical Properties of Aluminum and Its Alloys for Electrical Conductors. *Next Materials*, **9**; 101090

Reinke, G., R. K. Badibanga, M. S. Pestana, J. L. De Almeida Ferreira, J. A. Araujo, and C. R. Moreira da Silva (2020). Failure Analysis of Aluminum Wires in All Aluminum Alloy Conductors-AAAC. *Engineering Failure Analysis*, **107**; 104197

Riba, J. R., S. Bogarra, Á. Gómez-Pau, and M. Moreno-Eguilaz (2020). Uprating of Transmission Lines by Means of HTLS Conductors for a Sustainable Growth: Challenges, Opportunities, and Research Needs. *Renewable and Sustainable Energy Reviews*, **134**; 110334

Subedi, K. N., S. Bhandari, and S. F. P. Parker (2022). Electrical Conduction Processes in Aluminum: Defects and Phonons. *Physical Review B*, **105**(10); 104114

Volokitin, A. V., I. E. Volokitina, and G. G. Kurapov (2021). Effect of Extrusion and Drawing Deformation Method on Aluminum Alloy 6101 Structure and Mechanical Properties. *Metal Science and Heat Treatment*, **63**; 341–344

Zhu, Y. K., Q. Y. Chen, Q. Wang, H. Y. Yu, R. Li, J. P. Hou, and Z. F. Zhang (2018). Effect of Stress Profile on Microstructure Evolution of Cold-Drawn Commercially Pure Aluminum Wire Analyzed by Finite Element Simulation. *Journal of Materials Science & Technology*, **34**(7); 1214–1221

Zisman, A. A., V. V. Rybin, S. Van Boxel, M. Seefeldt, and B. Verlinden (2006). Equal Channel Angular Drawing of Aluminum Sheet. *Materials Science and Engineering: A*, **427**; 123–129

